CrossMark

ORIGINAL PAPER

First-principles calculations of equilibrium fractionation of O and Si isotopes in quartz, albite, anorthite, and zircon

Tian Qin[1,2] · Fei Wu[3] · Zhongqing Wu[1,2] · Fang Huang[3]

Abstract In this study, we used first-principles calculations based on density functional theory to investigate silicon and oxygen isotope fractionation factors among the most abundant major silicate minerals in granites, i.e., quartz and plagioclase (including albite and anorthite), and an important accessory mineral zircon. Combined with previous results of minerals commonly occurring in the crust and upper mantle (orthoenstatite, clinoenstatite, garnet, and olivine), our study reveals that the Si isotope fractionations in minerals are strongly correlated with SiO_4 tetrahedron volume (or average Si–O bond length). The ^{30}Si enrichment order follows the sequence of quartz > albite > anorthite > olivine ≈ zircon > enstatite > diopside, and the ^{18}O enrichment follows the order of quartz > albite > anorthite > enstatite > zircon > olivine. Our calculation predicts that measurable fractionation of Si isotopes can occur among crustal silicate minerals during high-temperature geochemical processes. This work also allows us to evaluate Si isotope fractionation between minerals and silicate melts with variable compositions. Trajectory for $\delta^{30}Si$ variation during fractional crystallization of silicate minerals was simulated with our calculated Si isotope fractionation factors between minerals and melts, suggesting the important roles of fractional crystallization to cause Si isotopic variations during magmatic differentiation. Our study also predicts that $\delta^{30}Si$ data of ferroan anorthosites of the Moon can be explained by crystallization and aggregation of anorthite during lunar magma ocean processes. Finally, O and Si isotope fractionation factors between zircon and melts were estimated based on our calculation, which can be used to quantitatively account for O and Si isotope composition of zircons crystallized during magma differentiation.

Communicated by Franck Poitrasson.

Tian Qin and Fei Wu are Co-first authors.

Keywords First-principles calculations · Zircon · Silicate minerals · O–Si isotope fractionation · Magma differentiation

✉ Fang Huang
  fhuang@ustc.edu.cn

  Zhongqing Wu
  wuzq10@ustc.edu.cn

[1] Laboratory of Seismology and Physics of Earth's Interior, School of Earth and Space Sciences, University of Science and Technology of China, Hefei, Anhui 230026, China

[2] National Geophysical Observatory at Mengcheng, Mengcheng, Anhui, China

[3] CAS Key Laboratory of Crust-Mantle Materials and Environments, School of Earth and Space Sciences, University of Science and Technology of China, Hefei 230026, Anhui, China

Introduction

Silicon and oxygen are the two most abundant elements in the Earth's crust, and silicon–oxygen polyhedrons form the skeleton of silicate minerals in the Earth. In the upper continental crust, petrogenesis of granite provides critical insights into the formation and evolution of the continental crust. As oxygen isotopes can be significantly fractionated in many geological processes, oxygen isotope geochemistry has been widely used to trace petrogenetic processes for

🌀 Springer

years (e.g., Eiler 2001 and references within). Due to the recent advances in Si isotope analytical techniques using MC–ICP–MS, Si isotope geochemistry has also been used to investigate granite formation (Savage et al. 2012). Specifically, an isotopically light Si signature may imply the involvement of sedimentary materials enriched in light Si isotopes into the source of granites, while slightly heavier Si isotope composition in granites could be due to magma differentiation (Savage et al. 2011).

For better understanding the O and Si isotopic variations during magmatism, it is crucial to obtain equilibrium fractionation factors of O and Si isotopes among rock-forming minerals. In the past few decades, O isotope equilibrium fractionation factors among silicate minerals have been extensively studied using theoretical and experimental methods (e.g., Zheng 1991, 1993; Chacko et al. 2001 and references therein). However, because equilibrium fractionation of Si isotopes between crustal silicate minerals at high temperature is small (~0.1 ‰ at 1000 °C) relative to the current analytical error (±0.07 ‰, 2SD, Poitrasson and Zambardi 2015), it is difficult to experimentally calibrate these small fractionations. This hampers the application of Si isotope fractionation to magmatic processes.

As one of the most important accessory minerals in crustal rocks, zircon is resistant to many geological processes after its formation, and the low diffusivities of elements (including oxygen) in zircon make it a exceptional archive to record the source magma compositions (Valley et al. 2003 and references therein). Therefore, the oxygen isotope composition of zircon is particularly useful in constraining source compositions and tracing magma evolution (e.g., Wei et al. 2002; Bindeman 2008). Regardless of extensive studies on O isotope fractionation between zircon and silicate minerals (Matsuhisa et al. 1979; Chiba et al. 1989; Clayton et al. 1989; Zheng 1993; Trail et al. 2009), different methods have produced discrepant results in fractionation factors. For example, $\Delta^{18}O_{zircon-quartz}$ was experimentally calibrated in Trail et al. (2009), which shows substantial deviation from the result obtained by the modified incremental methods (Zheng 1993) and other experimental methods (Matsuhisa et al. 1979; Chiba et al. 1989; Clayton et al. 1989). Furthermore, there is still no experimental work on Si equilibrium isotope fractionation factors between zircon and other silicate minerals.

Because of recent advances in computational chemistry, first-principles calculations based on density functional theory have become a reliable method to investigate equilibrium stable isotopic fractionations between minerals (e.g., Anbar et al. 2005; Méheut et al. 2007; Li et al. 2009; Li and Liu 2010, 2011; Schauble 2011; Huang et al. 2013; Méheut and Schauble 2014; Wu et al. 2015). Here, we calculate Si and O isotope fractionation factors between the dominant silicate minerals in granites (i.e., quartz, albite, and anorthite)

and zircon using the first-principles calculations method. Combining with a previous theoretical study on Si isotope fractionation between mafic minerals (orthoenstatite, clinoenstatite, diopside, and olivine from Huang et al. 2014), this work will investigate Si and O isotope fractionation factors among silicate minerals and melts, and examine Si and O isotope fractionation during fractional crystallization of silicate minerals during magmatic differentiation.

Methodology

Isotope fractionation factor α and reduced partition function ratio β

The mass-dependent equilibrium isotope fractionation arises from changes in phonon frequencies triggered by isotope substitution (Bigeleisen and Mayer 1947; Urey 1947). The element X isotope fractionation between phase A and phase B is always reported in the form of $10^3\ln\alpha_{A-B}$. α_{A-B} (defined as the ratio of isotope ratios: $\alpha_{A-B} = R_A/R_B$) is the isotope fractionation factor between phase A and phase B. If phase B is a perfect gas of X atoms, the isotope fractionation factor is defined as the reduced partition function ratio β (Richet et al. 1977). Therefore, α_{A-B} can be represented as $\alpha_{A-B} = \beta_A/\beta_B$.

For a crystal, the reduced partition function ratio β can be calculated based on the harmonic approximation and the Teller–Redlich rule:

$$\beta_A = \prod_i^{3N-3} \frac{u_{ih}}{u_{il}} \frac{e^{-\frac{1}{2}u_{ih}}}{(1-e^{-u_{ih}})} \frac{(1-e^{-u_{il}})}{e^{-\frac{1}{2}u_{il}}} \tag{1}$$

where $u_{il,h} = h\nu_{ih,l}/k_BT$, h, and l refer to the heavy and light isotope, respectively. T is the temperature in kelvin, h is Planck's constant, k_B is Boltzmann's constant, and ν_i is the vibrational frequency of the ith mode. This product runs over all 3 N-3 phonon modes (Bigeleisen and Mayer 1947; Urey 1947).

DFT calculation

Our calculation procedure was similar to that in previous studies (Anbar et al. 2005; Méheut et al. 2007; Rustad and Bylaska 2007; Li and Liu 2010; Schauble 2011). The local density approximations (LDA) was adopted as the exchange–correlation functional because the structure, thermodynamics properties, and phonon properties of minerals obtained from theoretical calculations based on the LDA match well with experimental observations (Perdew and Zunger 1981; Wentzcovitch 1991; Méheut et al. 2007; Huang et al. 2013). All calculations were performed using the Quantum ESPRESSO package in the framework of density functional theory, using

a plane-wave basis set to expand electronic wave functions, and adopting pseudopotential to describe the interaction between the valence electrons and the ionic core (Giannozzi et al. 2009). The plane-wave cutoff energy is 70 Rydberg. The pseudopotential for sodium was generated using the Vanderbilt method (Vanderbilt 1990) with valence configuration $2s^2 2p^6 3s^1$ and a 1.4 Bohr radii cutoff. The pseudopotential for zirconium was generated by Hartwigsen et al. (1998), and the other pseudopotentials are described in Huang et al. (2013). In each case, the structure was well optimized using variable cell shape molecular dynamics (Wentzcovitch 1991) before conducting any further calculations, and the total energy calculations and atomic positions were calculated with the residual force less than 5×10^{-4} Ry/Bohr. Electronic integration was performed by sampling the Brillouin zone with a $4 \times 4 \times 4$ k point grid for quartz, albite, and zircon, and $1 \times 1 \times 1$ k point grid for anorthite with the automatic scheme (Table S1).

Phonon frequencies were computed using the standard procedure, the dynamical matrices were calculated on a regular grid of *q*-vectors using density functional perturbation theory (Baroni et al. 2001) with a $4 \times 4 \times 4$ q-point grid for quartz and zircon, and a $1 \times 1 \times 1$ q-point grid for albite and anorthite then interpolated in a dense *q*-point grid to obtain the vibrational density of states of minerals (Table S1). Finally, the reduced partition function ratio β was obtained using the vibrational density of states according to the Eq. (1).

Results

Crystalline structures

The structures of all minerals optimized at the LDA level are shown in Fig. 1 with the emphasis on Si–O and Al–O tetrahedrons. The lattice parameters of all minerals in static calculations at the LDA level are slightly smaller than the experimental results by 0.5–1 % in lattice constants and 2–3 % in volume (Table 1). To further investigate the relationship of isotope fractionation and structure properties, the calculated average Si–O bond length and the SiO_4 tetrahedron volume are compared with experimental values in Fig. 4. As Fig. 4 shows, almost all the calculated bond length and volume are underestimated by ~2 % relative to the corresponding experimental value, which is common for calculation at the LDA level. The vibrational effect was not taken into account in the static calculations, which will generally increase the equilibrium volume by ~2 % at 0 GPa and 300 K (Wu and Wentzcovitch 2007; Wu et al. 2008; Huang et al. 2013). Therefore, we can expect that the calculated volume with the vibrational effect should agree well with the experimental data at ambient conditions

with an error of ~1 % (Wentzcovitch et al. 2010). Comparing with the structure predicted based on the general gradient approximation (GGA, Méheut et al. 2007; Méheut et al. 2009; Méheut and Schauble 2014), the LDA gives a smaller volume and bond length, but this does not affect the fractionation factor (or $10^3 ln\alpha_{A-B}$) because the systematic offsets of $10^3 ln\beta$ of minerals can be canceled out as $10^3 ln\alpha_{A-B} = 10^3 ln\beta_A - 10^3 ln\beta_B$ (Huang et al. 2013).

Calculated *β* and *α* factors

The *β* factors of O and Si isotopes were calculated from 300 to 2000 K at intervals of 5 K. The comparison between calculated vibrational frequencies of some newly calculated minerals and previous studies are shown in Fig. S1 and supplementary materials. $10^3 ln\beta$ and $10^3 ln\alpha$ are plotted as functions of third-order polynomials of temperature in Figs. 2 and 3, respectively (see fitted coefficients in Tables 2, 3). Figure 2 shows that the ^{18}O-enrichment order among these minerals follows the sequence quartz > albite > anorthite > enstatite > zircon > olivine, in good agreement with the data from previous theoretical and experimental studies on measurements of natural samples (Matsuhisa et al. 1979; Chiba et al. 1989; Clayton et al. 1989; Zheng 1993). The ^{30}Si-enrichment sequence follows the order of quartz > albite > anorthite > olivine ≈ zircon > enstatite > diopside, which is consistent with previous theoretical calculations (Méheut et al. 2009; Méheut and Schauble 2014) and isotopic analyses of natural minerals (Georg et al. 2007; Savage et al. 2011) (Fig. 3).

Discussion

O isotope fractionation factors

The O isotope fractionations among minerals have been widely used as a thermometer and isotopic tracer. The equilibrium fractionation factors between co-existing minerals are fundamental for application of oxygen isotope geochemistry. In this study, our calculated results agree well with previous literature values. For instance, the $10^3 ln\alpha_{O,qz-an}$ (Fig. 3a) is consistent with those predicted by the increment method (Zheng 1993), the experimental calibration by Clayton et al. (1989) and Matsuhisa et al. (1979), and $10^3 ln\alpha_{O,qz-ab}$ matches well with the value in Clayton et al. (1989). $10^3 ln\alpha_{O,qz-cl}$ and $10^3 ln\alpha_{O,qz-ol}$ (Fig. 3b, c) agree well with the results of a previous theoretical study in Méheut et al. (2009), despite the different approximation of exchange–correlation functional used in this study (LDA) and Méheut et al. (2009) (GGA). $10^3 ln\alpha_{O,qz-ol}$ in this study is also generally consistent with the values obtained by Chiba et al. (1989) and Zheng (1993) (Fig. 3c).

Fig. 1 Crystal structure of common rock-forming minerals and zircon, quartz (SiO_2), zircon ($ZrSiO_4$), low albite ($NaAlSi_3O_8$), anorthite ($CaAlSi_2O_8$), clinoenstatite ($Mg_2Si_2O_6$), diopside ($CaMgSi_2O_6$), olivine (Mg_2SiO_4), orthoenstatite ($Mg_2Si_2O_6$). The color of atoms: oxygen, *red*; silicon, *blue*; calcium, cyan; aluminum, light cyan (smaller than calcium cations in anorthite); magnesium, *brown*; zirconium, *green*; and sodium, *yellow*. The structures of orthoenstatite, diopside and olivine are from Huang et al. (2014). These minerals structure figures were generated using VESTA (Momma and Izumi 2008)
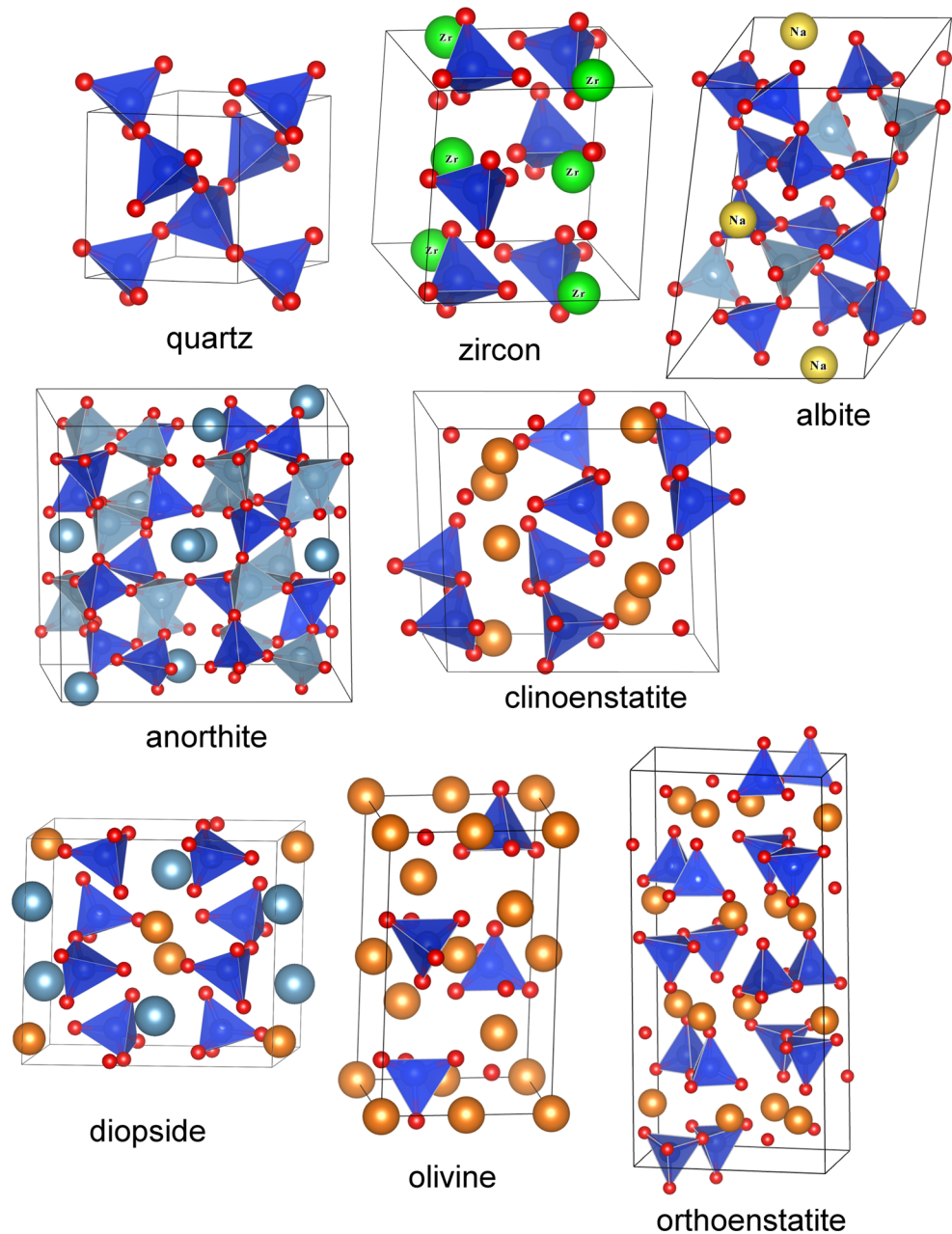
Although the O isotope fractionation factor between quartz and zircon ($10^3 \ln \alpha_{O,qz-zr} = \frac{10^6 A_{qz-zr}}{T^2}$) has been intensively studied by theoretical, empirical, and experimental methods, the A_{qz-zr} values vary from 1.36 to 3.25 in the literatures (Kieffer 1982; Zheng 1993; Chacko et al. 2001; King et al. 2001; Bindeman and Valley 2002; Krylov et al. 2002; Valley et al. 2003). Trail et al. (2009) discussed the possible processes that could cause discrepancy of $\Delta^{18}O_{qz-zr}$ in previous studies. For example, salt effects would influence the quartz–water or zircon–water equilibrium factor (Hu and Clayton 2003); or thermodynamic equilibrium between zircon and quartz cannot always be guaranteed during high-temperature experiments (Watson 1996). We

studied the equilibrium fractionation factor of oxygen isotopes between quartz and zircon using first-principles calculations. These results, shown in Fig. 3d and Table 3, are in good agreement with the recent literature values (Trail et al. 2009). Therefore, our work shows that the first-principles calculations provide an independent and reliable method to estimate oxygen isotope fractionation factors.

Si isotope fractionation factors among rock-forming minerals

The Si isotope fractionation factors calculated in this study together with literature values are summarized in Fig. 3e–h.

Fig. 2 **a** Calculated $10^3\ln\beta_O$ vs. $10^6/T^2$ for quartz (qz), albite (ab), anorthite (an), clinoenstatite (cl), diopside (dio), zircon (zr), and olivine (ol) at 0 GPa. **b** Calculated $10^3\ln\beta_{Si}$ vs. $10^6/T^2$ for qz, ab, an, cl, orthoenstatite (or), dio, zr and ol at static conditions. The $10^3\ln\beta_{Si}$ for olivine and zircon, and clinoenstatite and orthoenstatite are indistinguishable
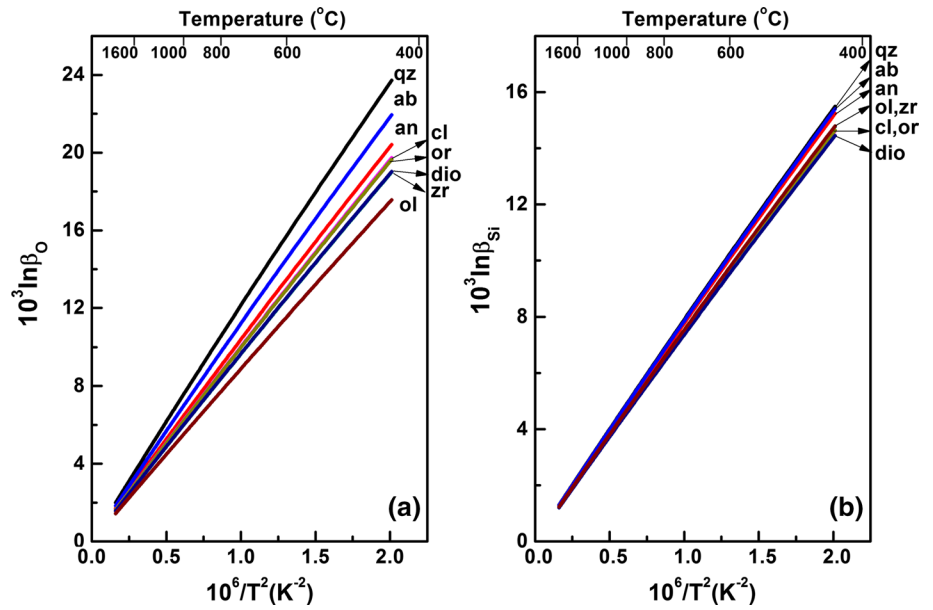

Fig. 3 **a–d** Comparison of calculated $10^3\ln\alpha_{qz\text{-}minerals}$ of oxygen isotopes in this study (solid lines) with experimental and theoretical values in the literature. The notations for different minerals are the same in caption of Fig. 2. The qz-an and qz-ab data C(1989) are from Clayton et al. (1989); the qz-an data M(1979) are from Matsuhisa et al. (1979); the qz-an, qz-ol, qz-zr data Z(1993) are from Zheng (1993); the qz-ol data Ch-(1989) are from Chiba et al. (1989); The qz-cl data M(2009) are from Méheut et al.(2009); the qz-zr data T(2009) are from Trail et al. (2009). **e–h** Calculated silicon equilibrium fractionation factors of $10^3\ln\alpha_{qz\text{-}minerals}$; the qz-ol, qz-cl data M(2009),M(2014) are from Méheut et al. (2009) and (Méheut and Schauble 2014)
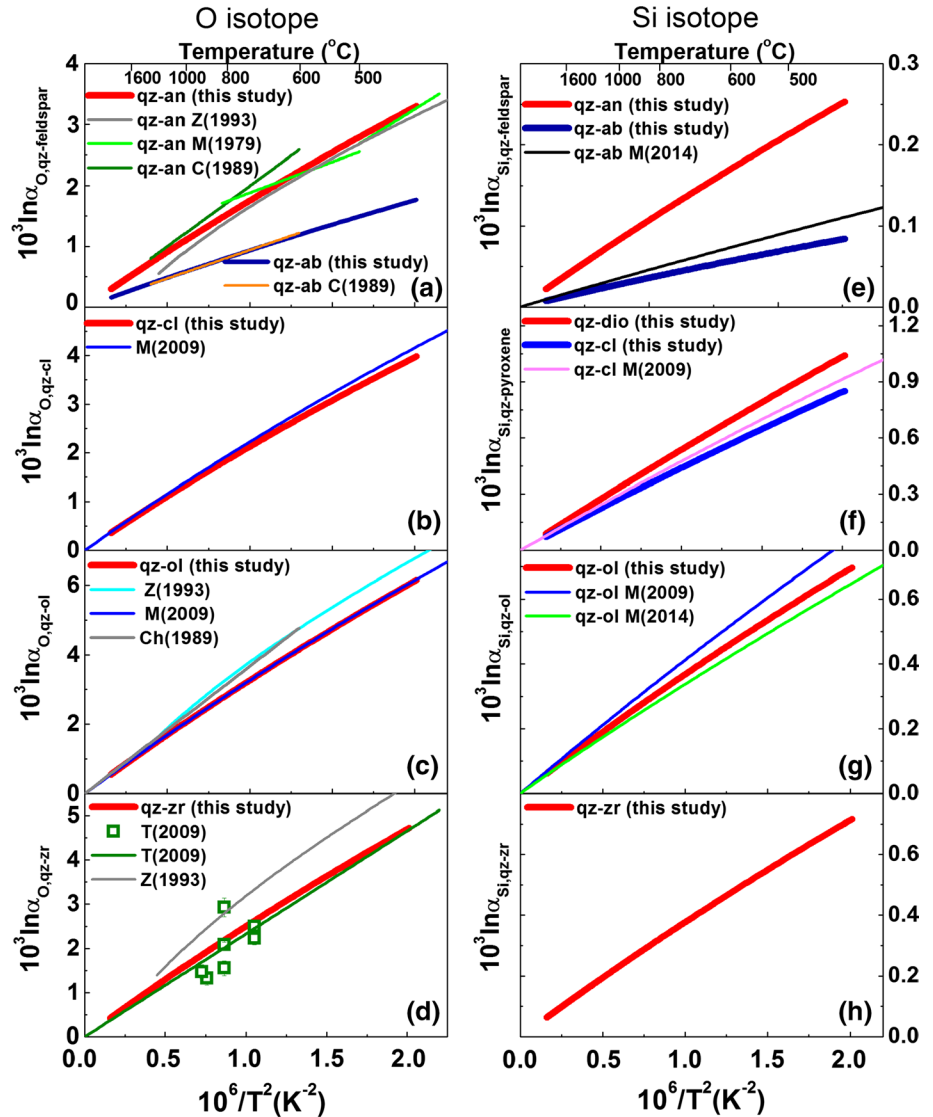
Table 1 Calculated static (without vibration effect) crystal lattice parameters at 0 GPa compared with experimental measurements at 0 GPa and 300 K

	a(Å)	b(Å)	c(Å)	α(°)	β(°)	γ(°)	V(Å³)	
Quartz	4.861	4.857	5.364			119.976	109.692	This work
	4.916	4.916	5.405			120.000	113.131	Experiment[a]
	−1.1 %	−1.2 %	−0.8 %			0.0 %	−3.0 %	Error
Albite	8.009	12.682	7.112	94.407	117.129	87.995	641.012	This work
	8.137	12.787	7.157	94.245	116.605	87.809	664.037	Experiment[b]
	−1.6 %	−0.8 %	−0.6 %	0.2 %	0.4 %	0.2 %	−3.5 %	Error
Anorthite	8.128	12.779	14.055	92.861	115.952	91.611	1308.925	This work
	8.173	12.869	14.165	93.113	115.913	91.261	1336.346	Experiment[c]
	−0.6 %	−0.7 %	−0.8 %	−0.3 %	0.0 %	0.4 %	−2.1 %	Error
Zircon	6.551		5.940				254.889	This work
	6.610		5.986				261.557	Experiment[d]
	−0.9 %		−0.8 %				−2.5 %	Error
Clinoenstatite	9.510	8.737	5.120		107.521		405.688	This work
	9.606	8.813	5.170		108.350		415.429	Experiment[e]
	−1.0 %	−0.9 %	−1.0 %		−0.8 %		−2.3 %	Error
Orthoenstatite	18.110	8.755	5.138				814.640	This work
	18.251	8.814	5.181				833.438	Experiment[f]
	−0.8 %	−0.7 %	−0.8 %				−2.3 %	Error
Diopside	9.689	8.828	5.211		105.263		430.010	This work
	9.745	8.899	5.251		105.630		438.532	Experiment[g]
	−0.6 %	−0.8 %	−0.8 %		−0.3 %		−1.9 %	Error
Olivine	4.738	10.115	5.941				284.713	This work
	4.752	10.192	5.978				289.529	Experiment[h]
	−0.3 %	−0.8 %	−0.6 %				−1.7 %	Error

Data sources for experimental studies: [a] Levien et al. (1980); [b] Downs et al. (1994); [c] Wainwright and Starkey (1971); [d] Finch et al. (2001); [e] Ohashi (1984); [f] Yang and Ghose (1995); [g] Cameron et al. (1973); [h] Kirfel et al. (2005)

Fig. 4 Comparison of calculated Si–O distance (**a**) and SiO₄ tetrahedron volume (**b**) with experimental values
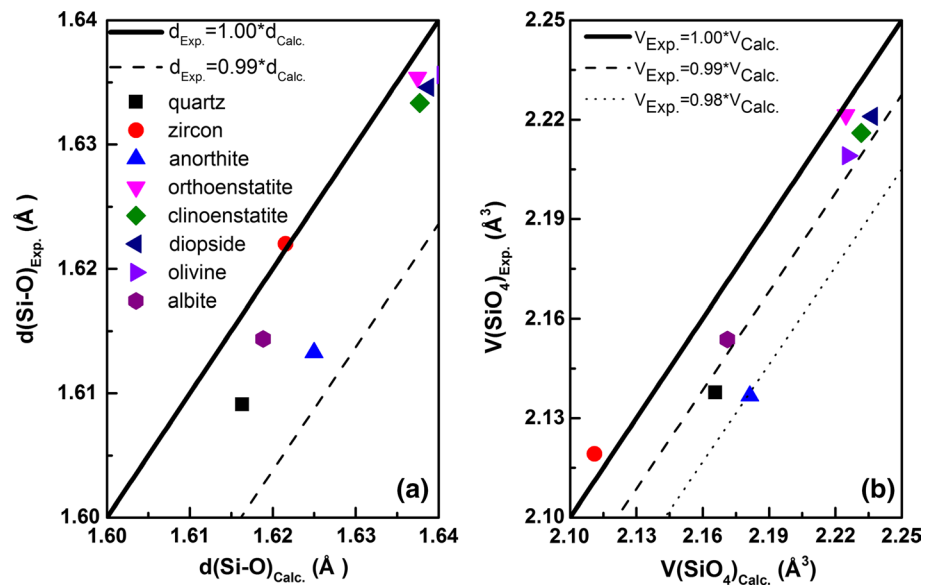
The silicon isotope fractionation factors among quartz, olivine, and enstatite in this study are consistent with calculations in Méheut et al. (2009) and Méheut and Schauble (2014). The fractionation factors calculated in this study agree with the variations in Si isotope compositions observed in natural samples. For instance, Savage et al.

Table 2 Calculated reduced partition function ratios of $^{18}O/^{16}O$ and $^{30}Si/^{28}Si$ ($10^3ln\beta$) for quartz, albite, anorthite, clinoenstatite, diopside, orthoenstatite, zircon, and olivine from 300 to 2000 K

Element	Minerals	a	b	c
$^{18}O/^{16}O$	Quartz	12.55277	−0.41976	0.01979
	Albite	11.55800	−0.35325	0.01557
	Anorthite	10.67645	−0.28680	0.01150
	Clinoenstatite	10.25586	−0.23959	0.00885
	Diopside	9.889990	−0.23237	0.00862
	Orthoenstatite	10.21370	−0.23955	0.00886
	Zircon	9.87055	−0.22965	0.00832
	Olivine	9.05093	−0.16847	0.00517
$^{30}Si/^{28}Si$	Quartz	8.12067	−0.22816	0.00947
	Albite	8.07297	−0.22462	0.00913
	Anorthite	7.97993	−0.21923	0.00875
	Clinoenstatite	7.66118	−0.20748	0.00822
	Diopside	7.56179	−0.20489	0.00815
	Orthoenstatite	7.65291	−0.20673	0.00817
	Zircon	7.71985	−0.20269	0.00782
	Olivine	7.72691	−0.20034	0.00729

$10^3ln\beta = ax + bx^2 + cx^3$, where $x = 10^6/T^2$. T is temperature in kelvin

[2012] observed small fractionation between quartz and feldspar ($\Delta^{30}Si_{qz-pl} \approx 0.10–0.14$ ‰) in S-type granites from the Cornubian batholith. This is consistent with the calculated $\Delta^{30}Si_{qz-pl}$, which is 0.05–0.15 ‰ at 700 °C in this study. At 1000 °C, the calculated $\Delta^{30}Si_{pl-ol}$ (0.16–0.22 ‰) and $\Delta^{30}Si_{ol-cpx}$ (0.11 ‰) also agree well with observations of the Skaergaard Intrusion ($\Delta^{30}Si_{pl-ol} = 0.23–0.27$ ‰ and $\Delta^{30}Si_{ol-cpx} = 0.08$ ‰) (Savage et al. 2011) and Cameroon Line spinel lherzolites ($\Delta^{30}Si_{ol-cpx} = 0.06–0.11$ ‰) (Georg et al. 2007).

Previous studies reveal that stable isotope fractionation in silicate minerals is related to the polymerization and chemical composition (Grant 1954; Méheut et al. 2009; Méheut and Schauble 2014). Our calculation further reveals that the Si isotope fractionation properties are obviously correlated with the SiO_4 tetrahedron volume. Grant (1954) pointed out that the polymerization of silicate would influence the internal vibrational frequencies of Si–O bonds. Although overestimating the fractionation magnitude, his work inferred that the silicate phases with high polymerization are enriched with heavier silicon isotopes. Further studies on Si isotope fractionation between lizardite and kaolinite with the same polymerization degree but different

Table 3 Comparison of oxygen and silicon isotope fractionation factors calculated in this study with literature data

Element		Formula	Data source
$^{18}O/^{16}O$	$10^3ln\alpha_{O,qz-an}$	$1.87632x − 0.13296x^2 + 0.0083x^3$	This study
		$1.99x$ (>600 °C)	Clayton et al. (1989)
		$−1.44 + 2.73x^{0.5} + 0.36x$ (0–1200 °C)	Zheng (1993)
		$−0.13 + 1.69x$ (400–500 °C)	Matsuhisa et al. (1979)
		$0.87 + 1.01x$ (500~800 °C)	Matsuhisa et al. (1979)
	$10^3ln\alpha_{O,qz-ab}$	$0.99476x − 0.0652x^2 + 0.00422x^3$	This study
		$0.94x$ (>600 °C)	Clayton et al. 1989
	$10^3ln\alpha_{O,qz-ol}$	$3.50184x − 0.25129x^2 + 0.01463x^3$	This study
		$0.001 + 3.482x − 0.2301x^2 + 0.01150x^3$	Méheut et al. (2009)
		$−2.09 + 4.95x^{0.5} + 0.93x$ (0–1200 °C)	Zheng, (1993)
		$3.67x$ (>600 °C)	Chiba et al. (1989)
	$10^3ln\alpha_{O,qz-cl}$	$2.2969x − 0.18017x^2 + 0.01094x^3$	This study
		$0.001 + 2.391x − 0.1747x^2 + 0.00914x^3$	Méheut et al. (2009)
	$10^3ln\alpha_{O,qz-zr}$	$2.68221x − 0.19012x^2 + 0.01147x^3$	This study
		$2.33(0.24)x$	Trail et al. (2009)
		$−1.79 + 4.26x^{0.5} + 0.72x$	Zheng (1993
$^{30}Si/^{28}Si$	$10^3ln\alpha_{Si,qz-ol}$	$0.39376x − 0.02783x^2 + 0.00218x^3$	This study
		$0.4343x − 0.0233x^2 + 0.0015x^3$	Méheut et al. (2009)
	$10^3ln\alpha_{Si,qz-cl}$	$0.45948x − 0.02068x^2 + 0.00125x^3$	This study
		$−0.0002 + 0.4972x − 0.0226x^2 + 0.0013x^3$	Méheut et al. (2009)
	$10^3ln\alpha_{Si,qz-or}$	$0.46776x − 0.02144x^2 + 0.00130x^3$	This study
	$10^3ln\alpha_{Si,qz-dio}$	$0.55888x − 0.02327x^2 + 0.00132x^3$	This study
	$10^3ln\alpha_{Si,qz-an}$	$0.14074x − 0.00893x^2 + 0.00072x^3$	This study
	$10^3ln\alpha_{Si,qz-ab}$	$0.04770x − 0.00354x^2 + 0.00034x^3$	This study
	$10^3ln\alpha_{Si,qz-zr}$	$0.40082x − 0.02547x^2 + 0.00165x^3$	This study

where $x = 10^6/T^2$. T is temperature in kelvin

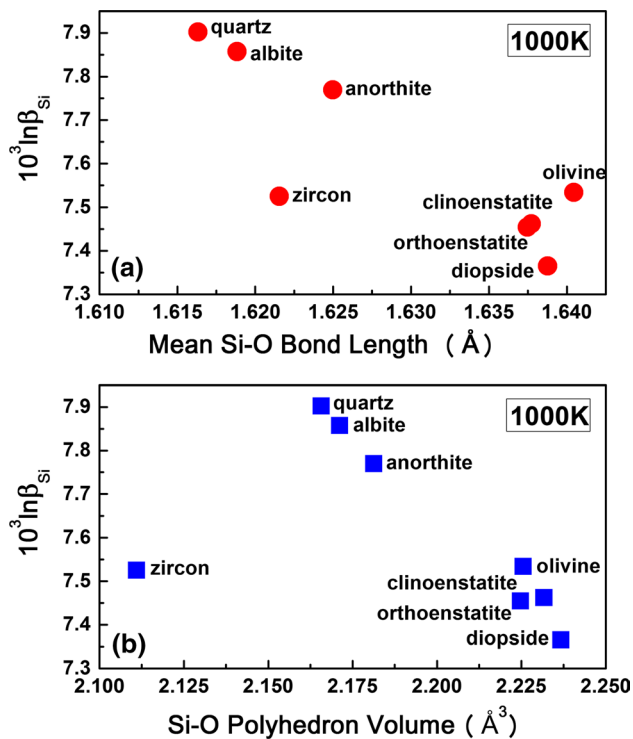**Fig. 5** $^{30}Si/^{28}Si$ fractionation factor at 1000 K vs. **a** average Si–O bond length and **b** volume of SiO_4 tetrahedron. Fitting equations: all minerals, $10^3 ln\beta_{Si} = -17.075*d(Si–O) + 35.432$ ($R^2 = 0.7096$), $10^3 ln\beta_{Si} = -2.3686*V(SiO_4) + 12.804$ ($R^2 = 0.2614$); all minerals except zircon, $10^3 ln\beta_{Si} = -20.224*d(Si–O) + 40.599$ ($R^2 = 0.9187$), $10^3 ln\beta_{Si} = -6.9193*V(SiO_4) + 22.880$ ($R^2 = 0.9779$); and all minerals except zircon and olivine, $10^3 ln\beta_{Si} = -22.657*d(Si–O) + 44.543$ ($R^2 = 0.9803$), $10^3 ln\beta_{Si} = -7.1602*V(SiO_4) + 23.401$ ($R^2 = 0.9906$)

fractionation properties suggest that the cations (especially aluminum) will affect the fractionation factor of Si isotopes (Méheut et al. 2009; Méheut and Schauble 2014).

Our results show a clear correlation between the fractionation of Si isotopes and the mean Si–O bond length or SiO_4 tetrahedron volume (Fig. 5). Generally, the shorter the mean Si–O bond length or smaller the SiO_4 tetrahedron volume of the mineral, the higher the $10^3 ln\beta$ and the greater enrichment of heavy Si isotopes. For instance, quartz and feldspar have higher polymerization degree and they are more enriched in heavy Si isotopes than pyroxene or olivine. However, for minerals with same polymerization degree (for example, quartz, albite, and anorthite), because they have different mean Si–O bond lengths and SiO_4 tetrahedron volumes, Si isotopes can also be fractionated among these minerals.

Figure 5 shows that $10^3 ln\beta_{Si}$ is well correlated with SiO_4 tetrahedron volume and mean Si–O bond length for most minerals. In Fig. 5a, olivine is slightly out of the main trend, which is similar to the results in Méheut and Schauble (2014), and zircon is a noticeable outlier with short Si–O bond length but relatively small β value. In Fig. 5b, olivine

fits well with the main trend defined by $10^3 ln\beta_{Si}$ and SiO_4 tetrahedron volume, while zircon is off from the trend due to a large distortion in the SiO_4 tetrahedron. The O–Si–O angles of SiO_4 tetrahedron of zircon are 97° and 116° instead of 109.47° of a normal angle, which likely results from repulsion between the Zr^{4+} and Si^{4+} cations (Finch and Hanchar 2003). Nonetheless, the good correlations of $10^3 ln\beta_{Si}$ with Si–O bond length and SiO_4 tetrahedron volume can be used to predict Si isotope fractionation of silicate minerals.

Si isotope fractionation between minerals and melts

Understanding isotope fractionations between minerals and melts is important for understanding isotopic variations in igneous rocks. Many studies on natural observations have shown measurable oxygen isotope fractionation between phenocrysts and lavas (Eiler et al. 1995; Baldridge et al. 1996; Eiler et al. 1997; Eiler 2000; Harris et al. 2000; Bindeman and Valley 2002). Recent works also revealed Si isotope fractionations between minerals and melts (Savage et al. 2011, 2012; Savage and Moynier 2013; Poitrasson and Zambardi 2015). However, there is still a lack of work to calibrate Si isotope fractionation between minerals and melts. Therefore, we estimate the controlling factors of Si isotope fractionations between minerals and melts based on our results and previous theoretical works (Méheut et al. 2009; Huang et al. 2014; Méheut and Schauble 2014).

Empirical relationship between oxygen isotope fractionations and the chemical composition of silicates was originally proposed by Garlick (1966), which was further confirmed by subsequent experimental and theoretical studies (Zheng 1991; Appora et al. 2003; Méheut et al. 2009). These works highlight chemical composition as the important controlling factor of oxygen fractionation in silicates. It is assumed that $10^3 ln\beta$ of $^{18}O/^{16}O$ for silicate melts are similar to the weighted sum of the $10^3 ln\beta$ of the minerals in proportion to their normative abundances in these melts (e.g., Eiler 2001; Zhao and Zheng 2003). Thus O isotope fractionations between minerals and melts could be estimated based on the dataset of O isotope fractionations among minerals. Many studies have successfully applied such method to illuminate O isotope variations of magmatic rocks and minerals (Eiler 2001; Zhao and Zheng 2003; Valley et al. 2003; Bindeman 2008; Trail et al. 2009).

The pioneering theoretical study of Grant (1954) has suggested that equilibrium isotope fractionation of Si should depend on the degree of polymerization of the SiO_4 tetrahedra in the silicate minerals. This work also implied the close relationship between Si isotope fractionation and chemical properties of silicates because the structure of silicates is mainly controlled by their compositions (Mysen and Virgo 1985; Huang 2006). Based on the electronegativity discrepancy among cations, recent first-principles

calculation studies emphasize the importance of the content of cation connected to SiO_4 tetrahedron in controlling Si fractionation properties of silicate (Méheut and Schauble 2014). Huang et al. (2014) showed that diopside (CaMgSi$_2$O$_6$) is enriched in lighter Si isotope relative to enstatite (MgSiO$_3$) (Fig. 2), which could be due to higher electropositivity of Ca cation than Mg cation, i.e., the electropositive cationic effect. Also, this study further suggests that $10^3\ln\alpha_{Si,ab-qz}$ and $10^3\ln\alpha_{Si,an-qz}$ are −0.057 and −0.171 ‰ at 600 °C, respectively, consistent with the results calculated from the empirical equation in Méheut and Schauble (2014) (−0.068 ‰ for $10^3\ln\alpha_{Si,ab-qz}$ and −0.205 ‰ for $10^3\ln\alpha_{Si,an-qz}$). Considering the existence of Al-O tetrahedra and related cations (such as Na, K, Ca) for charge balance in the structure of albite and anorthite, such consistency implies that Al cation shows the similar electropositive cationic effect on Si isotope fractionation in tectosilicates and phyllosilicates. However, for the cations connected to Al-O tetrahedra for charge balance, as they mainly affect the O connected with Al as an electron donor, such cations have little influence on the Si isotope fractionation of silicates. Consequently, we could infer that Si isotope fractionation properties and chemical composition are highly correlated for silicates, which are similar to the O isotope case.

Therefore, equilibrium isotope fractionation factors between minerals and melt can be calculated for melt with compositions ranging from basaltic to rhyolitic, based on the assumption that silicate melts have Si isotope fractionation factors equal to the weighted sum of those for their normative mineral compositions. Here we chose representative chemical compositions for magmatic rocks after Le Maitre (1976) as examples. The CIPW method is used to estimate normative mineral compositions of the melts (see details in Supplementary materials). The equilibrium Si isotope fractionation factor (cf. $10^3\ln\beta$) of main silicate minerals in magmatic rocks could be obtained with our calculation and a previous study (Huang et al. 2014). We further assume that Si isotope composition of orthoclase is same to albite because they have similar chemical compositions and crystal structures. Thus, we can get the $10^3\ln\beta$ of Si isotopes for the silicate melts through the weighted sum of $10^3\ln\beta$ for their normative mineral forms.

The estimated $10^3\ln\alpha_{melt-mineral}$ for Si isotopes is depicted in Fig. 6. As shown in Fig. 6a, mafic minerals such as olivine are enriched in light Si isotopes relative to the coexisting melt, which is consistent with the reported Si isotope variations in granulite facies xenoliths and Skaergaard mineral separates (Savage et al. 2011, 2013). Our calculation also predicts that feldspar is depleted in heavy Si isotopes while quartz is enriched in heavy Si isotopes relative to highly evolved melt (such as rhyolitic magma) (Fig. 6b), which is consistent with the observations for whole-rock and mineral separates of granites (Savage et al. 2012).
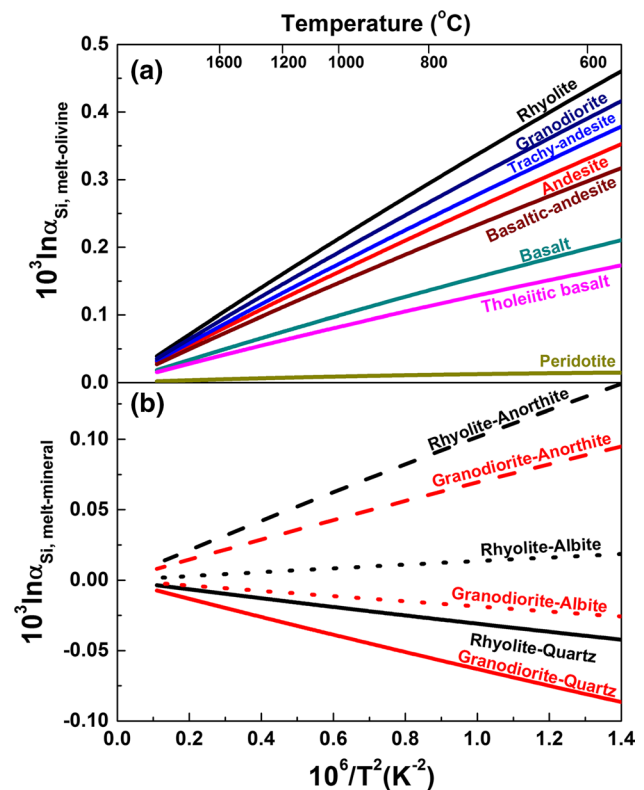

Fig. 6 Variations of Si isotope fractionation factors between minerals and melt with different compositions

Si isotope fractionation during magmatic differentiation

Measurements of terrestrial and lunar volcanic samples reveal that magmatic differentiation could preferentially enrich heavy Si isotopes in more differentiated rocks (Savage et al. 2011; Poitrasson and Zambardi 2015). It is proposed by Savage et al. (2011) that the removal of isotopically light minerals during fractional crystallization is the primary cause of Si isotope fractionation during magmatic differentiation. However, current model with constant Si isotope fractionation factors between melts and minerals do not match well the measured isotopic trend (Savage et al. 2011; Zambardi et al. 2014).

In this study, a variation of $\delta^{30}Si$ during fractional crystallization of silicate minerals was simulated using our estimated $\Delta^{30}Si_{minerals-melts}$. The software MELTS (Ghiorso and Sack 1995; Asimow and Ghiorso 1998; Gualda and Ghiorso 2014) based on thermodynamic modeling of phase equilibrium in magmatic systems was applied to determine the possible crystallization process. The elemental and Si isotopic compositions of Helka and Cedar Butte volcanic were chosen as initial magmatic compositions for the modeling (Table S2). The crystallization calculations were performed at two different pressures (1 Kbar and 4 Kbar),
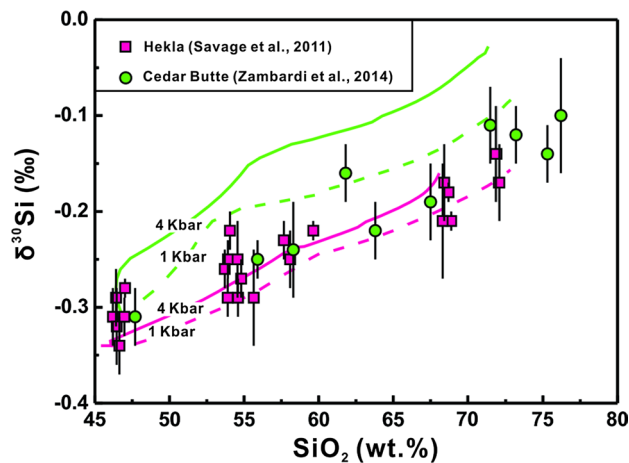
Fig. 7 Isotopic effects of Si associated with magma fractional crystallization. Crystallization path and isotopic fractionations for Helka volcanic suites (*red lines*) and Cedar Butte volcanic suites (*green lines*) under 1 Kbar (*dash lines*) and 4 Kbar (*solid lines*) were modeled by MELTS using typical starting melts compositions (Table S2). The Si isotope data as well as Si content of samples from Helka volcanic suites (*square*) and Cedar Butte volcanic suites (*round*) were also dotted here for comparing. See more details in text

Fig. 8 Calculated Si isotope composition of anorthite in equilibrium with lunar basalt at varying temperatures, assuming that $\delta^{30}Si$ value of lunar basalt is -0.30 ‰ from Poitrasson and Zambardi (2015). The chemical constitution of lunar basaltic magma is from Warren and Taylor (2014). The *shaded area* shows the $\delta^{30}Si$ values of ferroan anorthosite sample reported by Poitrasson and Zambardi (2015)

1 wt% water content, and fixed oxygen fugacity (QFM). The relative proportion and composition of crystallizing minerals as well as residual melt at each stage along the liquidus line of descent were provided by MELTS modeling. Then isotopic effects of fractionation steps of crystallization could be modeled with the equation:

$$\delta^{30}Si(\text{melt})_{j+1} = \delta^{30}Si(\text{melt})_j + \sum_i X_i \times 10^3 \ln \alpha_i(\text{T}) \quad (2)$$

where X_i are Si proportions of crystallizing minerals at each step j, and $10^3\ln\alpha_i(\text{T})$ are Si fractionation factors between melt and mineral depending on temperature and melt composition.

The modeling trends of $\delta^{30}Si(\text{melt})$ versus SiO_2 are presented with observations of Helka and Cedar Butte volcanic suites on Fig. 7. From the modeling results, it is clearly shown that $\delta^{30}Si(\text{melt})$ increases with the SiO_2 content increase in melts during fractional crystallization. Also as illustrated in Fig. 7, the trajectories of Si isotope trend at low-pressure condition consistently are located under the high-pressure models at same SiO_2 content. Such phenomenon may be caused by the promotion of early crystallization of olivine and spinel relative to pyroxene phases that inhibit the increase in $\delta^{30}Si(\text{melt})$ with SiO_2 content during early basalt differentiation at low pressure. The modeled fractional crystallization curves reproduce well the general trend observed for the Hekla suite (Savage et al. 2011), although in detail some samples plot significantly above when uncertainties are taken into account between 45 and 55 wt% SiO_2. The simulation trends show
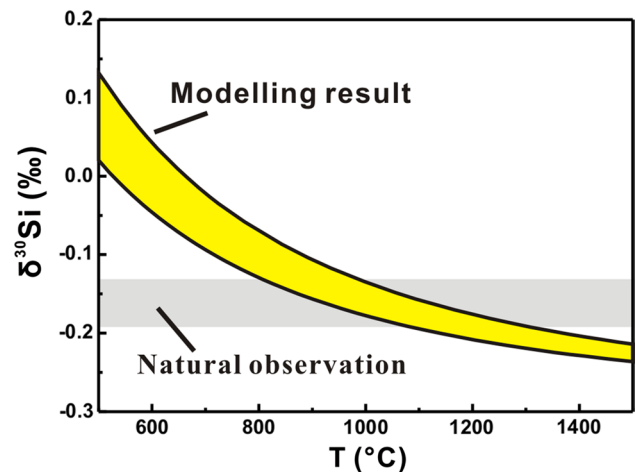
higher $\delta^{30}Si(\text{melt})$ at same SiO_2 content relative to the Cedar Butte volcanic suites (Zambardi et al. 2014), which mainly arises from the trajectory of $\delta^{30}Si$ increase with SiO_2 contents from about 45 to 55 wt%. Yet the modeled curves of Fig. 7 show the generally correlated increase in $\delta^{30}Si$ with SiO_2 due to fractional crystallization, which was presumed to be impossible according to Zambardi et al. (2014) when invariable silicon isotope fractionation factors between minerals and melts based on a small quantity of current observation were taken into account. Consequently, these modeling results highlight that crystallizing silicate minerals can fractionate Si isotopes during magmatic differentiation.

A recent study by Poitrasson and Zambardi (2015) revealed a clear positive relationship between $\delta^{30}Si$ and sum of felsic minerals abundance (silica, orthoclase, and plagioclase) for lunar rocks. In particular, the ferroan anorthosites, which consist almost entirely of anorthite, have heavier $\delta^{30}Si$ than other lunar samples, although its SiO_2 content is about the same as the others. It is generally acknowledged that ferroan anorthosites present crystallizing products of the lunar magma ocean (e.g., Elardo et al. 2011). We estimate Si isotope composition of anorthite in equilibrium with lunar basalt at various temperatures, assuming the $\delta^{30}Si$ value of lunar basalt is -0.30 ‰ (Poitrasson and Zambardi 2015). The chemical constitution of lunar basaltic magma is from Warren and Taylor (2014). The estimated $\delta^{30}Si$ values of anorthite and the measured $\delta^{30}Si$ of ferroan anorthosites are depicted in Fig. 8, showing that anorthites crystallized from the basaltic melt will have $\delta^{30}Si$ values similar to ferroan anorthosites at ~1050 °C.

Our study suggests that Si isotope signature of lunar ferroan anorthosites can be explained by crystallization and aggregation of anorthite from the basaltic melt.

Si and O isotope fractionation between zircon and silicate melt

Because zircon can resist physical and chemical breakdown during weathering, alteration, and metamorphism, O isotope composition of zircons has been widely used to investigate the composition and origin of their host rocks. Bindeman ([2008]) has modeled a normal-$\delta^{18}O$ differentiation array and pointed out that the O isotopic composition of melts that deviate from this trend might reflect assimilating of high $\delta^{18}O$ supracrustal materials or low $\delta^{18}O$ hydrothermally altered rocks. O isotope values of magmatic zircon from granites have been used to recognize such assimilation processes (e.g., Wei et al. [2002]). In addition, recent studies showed that Si isotope composition of magmatic rocks could indicate the contribution of sedimentary materials (Savage et al. [2011], [2012]; Poitrasson and Zambardi [2015]). Thus Si isotope signatures recorded by zircon could also be used as a proxy to trace crustal material recycling process. For this purpose, it is critical to calibrate Si and O isotope fractionation factors between melts and zircon ($\Delta^{30}Si_{melt-zircon}$ and $\Delta^{18}O_{melt-zircon}$). Previous work based on natural samples suggested that $\Delta^{18}O_{melt-zircon}$ is influenced by the melt composition (Valley et al. [2003]). Experimental calibration was also performed to obtain O isotope fractionation between minerals and melts with different compositions (Trail et al. [2009]). Here, we estimate $\Delta^{18}O_{melt-zircon}$ based on O isotope fractionation factors among minerals from our calculation and previous studies. Furthermore, because Si isotope fractionation factor of zircon was calculated, the $\Delta^{30}Si_{melt-zircon}$ can also be estimated.

To estimate the $\Delta^{30}Si_{melt-zircon}$ and $\Delta^{18}O_{melt-zircon}$ values, the assumption is made that reduced partition function ratios of $^{30}Si/^{28}Si$ and $^{18}O/^{16}O$ for silicate melts are similar to the weighed sum of the reduced partition function ratios of the minerals in proportion to their normative abundances in these melts. The CIPW normative mineral estimation is used to get the idealized mineralogy of the igneous rock. The $10^3\ln\beta_{mineral}$ of primary rock-forming minerals are from this study and previous studies (see the supplementary materials). The reduced partition function ratios obtained from different studies may introduce systematic deviations by using various methods. To avoid such systematic deviations, we use quartz as the reference mineral because quartz is one of the most studied minerals in the literature. After $\Delta^{30}Si_{melt-zircon}$ and $\Delta^{18}O_{melt-zircon}$ had been obtained, then Si and O isotope fractionation between zircon and silicate melt was calculated. We further provide an Excel program for the calculation procedure (see the supplementary
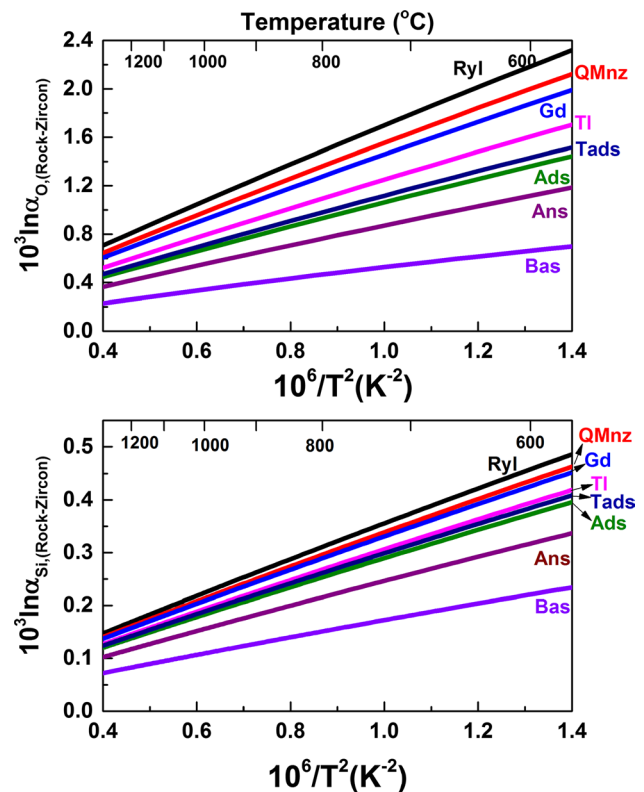

Fig. 9 Variations of Si and O isotope fractionation factors between zircon and rhyolite (Ryl), quartz-monzonite (QMnz), granodiorite (Gd), tonalite (Tl), andesite (Ads), trachy-andesite (Tads), basalt (Bas), and anorthosite (Ans)

materials) to estimate the $\Delta^{30}Si_{melt-zircon}$ and $\Delta^{18}O_{melt-zircon}$ with variable melt composition at geologically meaningful temperatures.

Figure [9] shows that Si and O isotopes can be significantly fractionated between zircon and melts, which are influenced by temperature and melt constitution. In particular, Si and O isotope fractionation between zircon and granitic melts could be up to 0.25~0.45 ‰ and 1.5–1.9 ‰ at the possible temperature range of granitic magmatism (600–900 °C) (Fig. [9]). Thus, when using zircons to estimate the Si and O isotope composition of their parental magma, the isotope offsets between the host magma and zircons should be considered.

Conclusions

This study calculates equilibrium Si and O isotope fractionation factors among rock-forming silicate minerals in the crust and upper mantle using first-principles calculations. Our result shows that the order of ^{30}Si enrichment is quartz > albite > anorthite > olivine ≈ zircon > enstatite > diopside. The sequence of ^{18}O

enrichment follows the order of quartz > albite > anorthite > enstatite > zircon > olivine. To the first order approximation, we predict that Si isotope fractionation in the minerals can be affected by polymerization extent and mineral structure, for instance, SiO_4 tetrahedron volume or average Si–O bond length.

We estimate Si isotope fractionation between minerals and silicate melts based on isotope fractionation factor among minerals. Combining MELTS software with the estimated fractionation factors, our work suggests that fractional crystallization of silicate minerals is a possible explanation of the Si isotope variations observed in Cedar Butte and Hekla igneous suites, although other processes such as magma mixing and/or assimilation might modify the Si isotope signature. And further refined modeling is required to perfectly match observed data. Silicon isotope signature of lunar ferroan anorthosites can also be explained by crystallization and aggregation of anorthite from basaltic melt during cooling of the lunar magma ocean. Finally, we estimate $\Delta^{30}Si_{melt-zircon}$ and $\Delta^{18}O_{melt-zircon}$ based on our calculation, which shows that zircon is enriched with light O and Si isotopes during crystallization. This would provide important insights into the validity of using O and Si isotope signatures in zircon to trace the source and magmatic processes of the host rocks.

References

Anba AD, Jarzecki AA, Spiro TG (2005) Theoretical investigation of iron isotope fractionation between Fe(H2O)63 + and Fe(H2O)62 + : implications for iron stable isotope geochemistry. Geochim Cosmochim Acta 69:825–837. doi:10.1016/j.gca.2004.06.012

Appora I, Eiler JM, Matthews A, Stolper EM (2003) Experimental determination of oxygen isotope fractionations between CO2 vapor and soda-melilite melt. Geochim Cosmochim Acta 67:459–471. doi:10.1016/S0016-7037(02)01090-6

Asimow PD, Ghiorso MS (1998) Algorithmic modifications extending MELTS to calculate subsolidus phase relations. Am Mineral 83:1127–1132. doi:10.2138/am-1998-9-1022

Baldridge WS, Sharp ZD, Reid KD (1996) Quartz-bearing basalts: Oxygen isotopic evidence for crustal contamination of continental mafic rocks. Geochim Cosmochim Acta 60:4765–4772. doi:10.1016/S0016-7037(96)00264-5

Baroni S, De Gironcoli S, Dal Corso A, Giannozzi P (2001) Phonons and related crystal properties from density-functional perturbation theory. Rev Mod Phys 73:515–562. doi:10.1103/RevModPhys.73.515

Bigeleisen J, Mayer MG (1947) Calculation of equilibrium constants for isotopic exchange reactions. J Chem Phys 15:261. doi:10.1063/1.1746492

Bindeman I (2008) Oxygen isotopes in mantle and crustal magmas as revealed by single crystal analysis. Rev Mineral Geochem 69:445–478. doi:10.2138/rmg.2008.69.12

Bindeman I, Valley J (2002) Oxygen isotope study of the Long Valley magma system, California: isotope thermometry and convection in large silicic magma bodies. Contrib Mineral Petrol 144:185–205. doi:10.1007/s00410-002-0371-8

Cameron M, Sueno S, Prewitt CT, Papike JJ (1973) High-temperature Crystal-chemistry of Acmite, Diopside, Hedenbergite, Jadeite, Spodumene, and Ureyite. Am Mineral 58:594–618

Chacko T, Cole DR, Horita J (2001) Equilibrium oxygen, hydrogen and carbon isotope fractionation factors applicable to geologic systems. Rev Mineral Geochemistry 43:1–81. doi:10.2138/gsrmg.43.1.1

Chiba H, Chacko T, Clayton RN, Goldsmith JR (1989) Oxygen isotope fractionations involving diopside, forsterite, magnetite, and calcite: Application to geothermometry. Geochim Cosmochim Acta 53:2985–2995. doi:10.1016/0016-7037(89)90174-9

Clayton RN, Goldsmith JR, Mayeda TK (1989) Oxygen isotope fractionation in quartz, albite, anorthite and calcite. Geochim Cosmochim Acta 53:725–733. doi:10.1016/0016-7037(89)90015-X

Downs RT, Hazen RM, Finger LW (1994) The high-pressure crystal-chemistry of low albite and the origin of the pressure dependency of Al-Si ordering. Am Mineral 79:1042–1052

Eiler JM (2000) Oxygen isotope geochemistry of oceanic-arc lavas. J Petrol 41:229–256. doi:10.1093/petrology/41.2.229

Eiler JM (2001) Oxygen isotope variations of basaltic lavas and upper mantle rocks. Rev Mineral Geochem 43:319–364. doi:10.2138/gsrmg.43.1.319

Eiler JM, Farley KA, Valley JW et al (1995) Oxygen isotope evidence against bulk recycled sediment in the mantle sources of Pitcairn Island lavas. Nature 377:138–141. doi:10.1038/377138a0

Eiler JM, Farley KA, Valley JW et al (1997) Oxygen isotope variations in ocean island basalt phenocrysts. Geochim Cosmochim Acta 61:2281–2293. doi:10.1016/S0016-7037(97)00075-6

Elardo SM, Draper DS, Shearer CK (2011) Lunar Magma Ocean crystallization revisited: bulk composition, early cumulate mineralogy, and the source regions of the highlands Mg-suite. Geochim Cosmochim Acta 75:3024–3045. doi:10.1016/j.gca.2011.02.033

Finch RJ, Hanchar JM (2003) Structure and chemistry of zircon and zircon-group minerals. Rev Mineral Geochem 53:1–25

Finch RJ, Hanchar JM, Hoskin PWO, Burns PC (2001) Rare-earth elements in synthetic zircon: part 2. A single-crystal X-ray study of xenotime substitution. Am Mineral 86:681–689

Garlick GD (1966) Oxygen isotope fractionation in igneous rocks. Earth Planet Sci Lett 1:361–368. doi:10.1016/0012-821X(66)90026-4

Georg RB, Halliday AN, Schauble EA, Reynolds BC (2007) Silicon in the earth's core. Nature 447:1102–1106. doi:10.1038/nature05927

Ghiorso MS, Sack RO (1995) Chemical mass transfer in magmatic processes IV. A revised and internally consistent thermodynamic model for the interpolation and extrapolation of liquid-solid equilibria in magmatic systems at elevated temperatures and pressures. Contrib Mineral Petrol 119:197–212. doi:10.1007/BF00307281

Giannozzi P, Baroni S, Bonini N et al (2009) QUANTUM ESPRESSO: a modular and open-source software project for quantum simulations of materials. J Phys: Condens Matter 21:395502

Grant FS (1954) The geological significance of variations in the abundances of the isotopes of silicon in rocks. Geochim Cosmochim Acta 5:225–242. doi:10.1016/0016-7037(54)90046-0

Gualda GAR, Ghiorso MS (2014) Phase-equilibrium geobarometers for silicic rocks based on rhyolite-MELTS. Part 1: principles, procedures, and evaluation of the method. Contrib Mineral Petrol. doi:10.1007/s00410-014-1033-3

Harris C, Smith HS, le Roex AP (2000) Oxygen isotope composition of phenocrysts from Tristan da Cunha and Gough Island lavas: variation with fractional crystallization and evidence for assimilation. Contrib Mineral Petrol 138:164–175. doi:10.1007/s004100050015

Hartwigsen C, Goedecker S, Hutter J (1998) Relativistic separable dual-space Gaussian pseudopotentials from H to Rn. Phys Rev B 58:3641–3662. doi:10.1103/PhysRevB.58.3641

Hu GX, Clayton RN (2003) Oxygen isotope salt effects at high pressure and high temperature and the calibration of oxygen isotope geothermometers. Geochim Cosmochim Acta 67:3227–3246

Huang F (2006) Effect of melt structure on trace-element partitioning between clinopyroxene and silicic, alkaline, aluminous melts. Am Mineral 91:1385–1400. doi:10.2138/am.2006.1909

Huang F, Chen L, Wu Z, Wang W (2013) First-principles calculations of equilibrium Mg isotope fractionations between garnet, clinopyroxene, orthopyroxene, and olivine: implications for Mg isotope thermometry. Earth Planet Sci Lett 367:61–70. doi:10.1016/j.epsl.2013.02.025

Huang F, Wu Z, Huang S, Wu F (2014) First-principles calculations of equilibrium silicon isotope fractionation among mantle minerals. Geochim Cosmochim Acta 140:509–520. doi:10.1016/j.gca.2014.05.035

Kieffer SW (1982) Thermodynamics and lattice vibrations of minerals: 5. Applications to phase equilibria, isotopic fractionation, and high-pressure thermodynamic properties. Rev Geophys 20:827–849. doi:10.1029/RG020i004p00827

King EM, Valley JW, Davis DW, Kowallis BJ (2001) Empirical determination of oxygen isotope fractionation factors for titanite with respect to zircon and quartz. Geochim Cosmochim Acta 65:3165–3175. doi:10.1016/S0016-7037(01)00639-1

Kirfel A, Lippmann T, Blaha P et al (2005) Electron density distribution and bond critical point properties for forsterite, Mg2 SiO4, determined with synchrotron single crystal X-ray diffraction data. Phys Chem Miner 32:301–313. doi:10.1007/s00269-005-0468-5

Krylov DP, Zagnitko VN, Hoernes S et al (2002) Oxygen isotope fractionation between zircon and water: experimental determination and comparison with quartz-zircon calibrations. Eur J Mineral 14:849–853

Le Maitre RW (1976) The chemical variability of some common igneous rocks. J Petrol 17:589–598. doi:10.1093/petrology/17.4.589

Levien L, Prewir CT, Weidner DJ et al (1980) Structure and elastic properties of quartz at pressure. Am Mineral 65:920–930

Li XF, Liu Y (2010) First-principles study of Ge isotope fractionation during adsorption onto Fe(III)-oxyhydroxide surfaces. Chem Geol 278:15–22. doi:10.1016/j.chemgeo.2010.05.008

Li X, Liu Y (2011) Equilibrium Se isotope fractionation parameters: a first-principles study. Earth Planet Sci Lett 304:113–120. doi:10.1016/j.epsl.2011.01.022

Li X, Zhao H, Tang M, Liu Y (2009) Theoretical prediction for several important equilibrium Ge isotope fractionation factors and geological implications. Earth Planet Sci Lett 287:1–11. doi:10.1016/j.epsl.2009.07.027

Matsuhisa Y, Goldsmith JR, Clayton RN (1979) Oxygen isotopic fractionation in the system quartz-albite-anorthite-water. Geochim Cosmochim Acta 43:1131–1140. doi:10.1016/0016-7037(79)90099-1

Méheut M, Schauble EA (2014) Silicon isotope fractionation in silicate minerals: insights from first-principles models of phyllosilicates, albite and pyrope. Geochim Cosmochim Acta 134:137–154. doi:10.1016/j.gca.2014.02.014

Méheut M, Lazzeri M, Balan E, Mauri F (2007) Equilibrium isotopic fractionation in the kaolinite, quartz, water system: prediction from first-principles density-functional theory. Geochim Cosmochim Acta 71:3170–3181. doi:10.1016/j.gca.2007.04.012

Méheut M, Lazzeri M, Balan E, Mauri F (2009) Structural control over equilibrium silicon and oxygen isotopic fractionation: a first-principles density-functional theory study. Chem Geol 258:28–37. doi:10.1016/j.chemgeo.2008.06.051

Mysen BO, Virgo D (1985) Structure and properties of fluorine-bearing aluminosilicate melts: the system Na2O-Al2O3-SiO2-F at 1 atm. Contrib Mineral Petrol 91:205–220. doi:10.1007/BF00413348

Ohashi Y (1984) Polysynthetically-twinned structures of enstatite and wollastonite. Phys Chem Miner 10:217–229. doi:10.1007/BF00309314

Perdew JP, Zunger A (1981) Self-interaction correction to density-functional approximations for many-electron systems. Phys Rev B 23:5048

Poitrasson F, Zambardi T (2015) An earth-moon silicon isotope model to track silicic magma origins. Geochim Cosmochim Acta 167:301–312. doi:10.1016/j.gca.2015.07.005

Richet P, Bottinga Y, Javoy M (1977) A review of hydrogen, carbon, nitrogen, oxygen, sulphur, and chlorine stable isotope fractionation among gaseous molecules. Annu Rev Earth Planet Sci 5:65–110. doi:10.1146/annurev.ea.05.050177.000433

Rustad JR, Bylaska EJ (2007) Ab initio calculation of isotopic fractionation in B(OH)3(aq) and BOH4-(aq). J Am Chem Soc 129:2222–2223. doi:10.1021/ja0683335

Savage PS, Moynier F (2013) Silicon isotopic variation in enstatite meteorites: clues to their origin and Earth-forming material. Earth Planet Sci Lett 361:487–496. doi:10.1016/j.epsl.2012.11.016

Savage PS, Georg RB, Williams HM et al (2011) Silicon isotope fractionation during magmatic differentiation. Geochim Cosmochim Acta 75:6124–6139. doi:10.1016/j.gca.2011.07.043

Savage PS, Georg RB, Williams HM et al (2012) The silicon isotope composition of granites. Geochim Cosmochim Acta 92:184–202. doi:10.1016/j.gca.2012.06.017

Savage PS, Georg RB, Williams HM, Halliday AN (2013) Silicon isotopes in granulite xenoliths: insights into isotopic fractionation during igneous processes and the composition of the deep continental crust. Earth Planet Sci Lett 365:221–231. doi:10.1016/j.epsl.2013.01.019

Schauble EA (2011) First-principles estimates of equilibrium magnesium isotope fractionation in silicate, oxide, carbonate and hexaaquamagnesium(2 +) crystals. Geochim Cosmochim Acta 75:844–869. doi:10.1016/j.gca.2010.09.044

Trail D, Bindeman IN, Watson EB, Schmitt AK (2009) Experimental calibration of oxygen isotope fractionation between quartz and zircon. Geochim Cosmochim Acta 73:7110–7126. doi:10.1016/j.gca.2009.08.024

Urey HC (1947) The thermodynamic properties of isotopic substances. J Chem Soc. doi:10.1039/jr9470000562

Valley JW, Bindeman IN, Peck WH (2003) Empirical calibration of oxygen isotope fractionation in zircon. Geochim Cosmochim Acta 67:3257–3266. doi:10.1016/S0016-7037(03)00090-5

Vanderbilt D (1990) Soft self-consistent pseudopotentials in a generalized eigenvalue formalism. Phys Rev B 41:7892

Wainwright JE, Starkey J (1971) A refinement of the structure of anorthite*,1. Zeitschrift für Krist 133:75–84. doi:10.1524/zkri.1971.133.133.75

Warren PH, Taylor GJ (2014) The Moon. In: Treatise on Geochemistry. Elsevier, pp 213–250

Watson EB (1996) Dissolution, growth and survival of zircons during crustal fusion: kinetic principals, geological models and implications for isotopic inheritance. Trans R Soc Edinb Earth Sci 87:43–56. doi:10.1017/S0263593300006465

Wei C-S, Zheng Y-F, Zhao Z-F, Valley JW (2002) Oxygen and neodymium isotope evidence for recycling of juvenile crust in northeast China. Geology 30:375. doi:10.1130/0091-7613(2002)030<0375:OANIEF>2.0.CO;2

Wentzcovitch RM (1991) Invariant molecular-dynamics approach to structural phase transitions. Phys Rev B 44:2358

Wentzcovitch RM, Yonggang GY, Wu Z (2010) Thermodynamic properties and phase relations in mantle minerals investigated by first principles quasiharmonic theory. Rev Mineral Geochem 71:59–98

Wu Z, Wentzcovitch RM (2007) Vibrational and thermodynamic properties of wadsleyite: A density functional study

Wu Z, Wentzcovitch RM, Umemoto K, et al (2008) Pressure-volume-temperature relations in MgO: An ultrahigh pressure-temperature scale for planetary sciences applications

Wu Z, Huang F, Huang S (2015) Isotope fractionation induced by phase transformation: first-principles investigation for Mg2SiO4. Earth Planet Sci Lett 409:339–347. doi:10.1016/j.epsl.2014.11.004

Yang HX, Ghose S (1995) High-Temperature Single-Crystal X-Ray-Diffraction Studies of the Ortho-Proto Phase-Transition in Enstatite, Mg2si2o6 at 1360 K. Phys Chem Miner 22:300–310

Zambardi T, Lundstrom CC, Li X, McCurry M (2014) Fe and Si isotope variations at Cedar Butte volcano; insight into magmatic differentiation. Earth Planet Sci Lett 405:169–179. doi:10.1016/j.epsl.2014.08.020

Zhao ZF, Zheng YF (2003) Calculation of oxygen isotope fractionation in magmatic rocks. Chem Geol 193:59–80

Zheng Y-F (1991) Calculation of oxygen isotope fractionation in metal oxides. Geochim Cosmochim Acta 55:2299–2307. doi:10.1016/0016-7037(91)90105-E

Zheng YF (1993) Calculation of oxygen isotope fractionation in anhydrous silicate minerals. Geochim Cosmochim Acta 57:1079–1091. doi:10.1016/0016-7037(93)90042-U